Available online at www.sciencedirect.com
ScienceDirect
International Journal of Heat and Mass Transfer 50 (2007) 3315–3328
International Journal of HEAT and MASS TRANSFER
www.elsevier.com/locate/ijhmt

Simulating oscillatory flows in Rayleigh–Bénard convection using the lattice Boltzmann method

P.-H. Kao, R.-J. Yang *

Department of Engineering Science, National Cheng Kung University, Tainan 70101, Taiwan

Received 17 August 2006; received in revised form 26 January 2007
Available online 29 March 2007

Abstract

Rayleigh–Bénard convection is a fundamental phenomenon found in many atmospheric and industrial applications. Many numerical methods have been applied to analyze this problem, including the lattice Boltzmann method (LBM), which has emerged as one of the most powerful computational fluid dynamics (CFD) methods in recent years. Using a simple LB model with the Boussinesq approximation, this study investigates the 2D Rayleigh–Bénard problem from the threshold of the primary instability with a theoretical value of critical Rayleigh number $Ra_c = 1707.76$ to the regime near the flow bifurcation to the secondary instability. Since the fluid of LBM is compressible, an appropriate velocity scale for natural convection, i.e. $V \equiv \sqrt{\beta g_y \Delta T H}$, is carefully chosen at each value of the Prandtl number to ensure that the simulations satisfy the incompressible condition. The simulation results show that periodic unsteady flows take place at certain Prandtl numbers with an appropriate Rayleigh number. Furthermore, the Nusselt number is found to be relatively insensitive to the Prandtl number in the current simulation ranges of $0.71 \leqslant Pr \leqslant 70$ and $Ra \leqslant 10^5$. Finally, the relationship between the Nusselt number and the Rayleigh number is also investigated.

Keywords: Rayleigh–Bénard convection; Natural convection; Lattice Boltzmann method (LBM); Computational fluid dynamics (CFD)

1. Introduction

Due to its practical importance in many general science and engineering applications, Rayleigh–Bénard convection has been the subject of many theoretical, experimental, and numerical studies. Since Rayleigh–Bénard convection presents the evolution from the stationary state to the fully developed turbulent regime with many different flow patterns and sequences of bifurcations, it is widely investigated as the problems of different transition mechanisms in hydrodynamics [1–4].

In Rayleigh–Bénard convection, the primary instability, which represents a transition from diffusive thermal conduction to stationary time-independent steady convection with a structure of steady 2D rolls, occurs at a critical Rayleigh number of $Ra_c = 1707.76$ for the case of no-slip boundary conditions imposed on solid walls. The value of this critical Rayleigh number is independent of the Prandtl number. However, as the Rayleigh number increases, a bifurcation to a time-dependent flow structure with a single-frequency periodic state is observed, namely the secondary instability. This transition to the secondary instability is strongly dependent on the Prandtl number. Moreover, as the Rayleigh number is increased further, two-frequency quasi-periodic flow is generated from the single-frequency oscillatory state and the flow finally transits to a chaotic state in the fully developed turbulent regime. Early experimental results for the transition to turbulence in Rayleigh–Bénard convection were presented by Krishnamurti [5]. More recently, various studies have employed numerical methods to investigate the bifurcations to oscillatory flow in Rayleigh–Bénard convection [6–10]. In these studies, the authors presented numerical results for symmetry-breaking solutions of flow

* Corresponding author. Tel.: +886 6 200 2724; fax: +886 6 276 6549.
E-mail address: rjyang@mail.ncku.edu.tw (R.-J. Yang).

0017-9310/$ - see front matter © 2007 Elsevier Ltd. All rights reserved.
doi:10.1016/j.ijheatmasstransfer.2007.01.035

Nomenclature

a_c	critical wave number for primary instability in Rayleigh–Bénard convection
AR	aspect ratio
c_i	microscopic particle velocity in each lattice link i
c_s	speed of sound
f	distribution function for the flow field
f_D	reference thermal diffusive frequency
f_P	induced oscillatory frequency
f^*	dimensionless frequency ratio
g	distribution function for the temperature field
g_y	acceleration of gravity in the y-direction
H	vertical height of the computational domain
J_i	momentum input from the buoyant body force in each lattice link i
L	horizontal length of the computational domain
Nu	Nusselt number
$\overline{Nu}$	average Nusselt number
Pr	Prandtl number
r	power value for the power law: $Nu \propto Ra^r$
Ra	Rayleigh number
Ra_c	critical Rayleigh number for primary instability in Rayleigh–Bénard convection
T	temperature
t	macroscopic time
t_D	reference thermal diffusive time scale: $t_D = H^2/\alpha$
t_p	time of period for the induced oscillatory flow
u_A	macroscopic flow velocities, where subindex A is the components of Cartesian coordinates
V	characteristic velocity of natural convection, $V \equiv \sqrt{\beta g_y \Delta T H}$

Greek symbols

α	thermal diffusivity
β	expansion coefficient: $\beta \equiv -1/\rho_{ref}(\partial\rho/\partial T)_P$
ℓ	length scale according to specific case of natural convection problems
ΔT	temperature difference
Δt	time interval (step) of LBM
v	kinetic viscosity
ρ	fluid density
τ_D	relaxation time for the temperature field
τ_v	relaxation time for the flow field

bifurcations and estimated the Rayleigh number for the oscillatory flows occurring at Prandtl numbers of approximately $Pr = 6$.

The kinetic-based lattice Boltzmann method (LBM) is a powerful numerical technique for simulating fluid flows and modeling the physics in fluids [11–15]. However, the application of LBM to heat transfer problems has not achieved great success for the thermal models due to the severe numerical instability caused by breaking the isothermal condition [15]. Various numerical simulations have been performed using different thermal LB models or Boltzmann-based schemes to investigate 2D Rayleigh–Bénard convection [16–19]. Although the results provided by these studies for stationary convection are in good agreement with the data presented in [2], the flow bifurcation to the secondary instability at different Prandtl numbers was not examined and discussed by thermal LB models.

The present study employs a simple thermal LB model with the Boussinesq approximation to simulate the oscillatory flows of the secondary instability in 2D Rayleigh–Bénard convection. The present study also investigates the structure of the oscillatory flow for this natural convection problem using the simple LB model. In this study, the thermal LB model is simplified by neglecting the viscous thermal dissipation for incompressible flows. However, the compressibility of LB fluids must be taken into consideration in the applications of compressible codes to the incompressible limit, as reported in [16,17,20]. Therefore, a correction procedure is applied to obtain an appropriate characteristic velocity of natural convection, i.e. $V \equiv \sqrt{\beta g_y \Delta T H}$, for different Prandtl numbers to ensure that the incompressible condition is satisfied. Furthermore, the simulations are restricted to the Prandtl number range of $0.71 \leqslant Pr \leqslant 70$ and to the Rayleigh numbers of $Ra \leqslant 10^5$ to ensure numerical stability and computational accuracy. Having explored the oscillatory flows of the secondary instability in 2D Rayleigh–Bénard convection, the relationship between the Nusselt number and the Rayleigh number is investigated for Prandtl numbers in the range of $0.71 \leqslant Pr \leqslant 70$.

2. Numerical method

2.1. Lattice Boltzmann model

In investigating the natural convection problem, this study neglects the viscous heat dissipation in applications of incompressible flow such that a simple lattice Boltzmann method can be used. The LB model comprises two distribution functions, f and g, for the flow filed and the temperature field, respectively. The density and the temperature distribution functions, f and g, are defined as the probability of particles at site x at time t moving with the particle velocity c_i during the time interval Δt in each lattice direction (link) i. The same model was proposed in [21,22]. The two distribution functions obey their respective lattice Boltzmann transport equations with the single relaxation Bhatnagar–Gross–Krook (BGK) approximation, i.e.

$$f_i(x+c_i\Delta t, t+\Delta t) - f_i(x,t) = \frac{\Delta t}{\tau_v}[f_i^{\mathrm{eq}}(x,t) - f_i(x,t)] + \dot{J}_i$$

for the flow field (1)

$$g_i(x+c_i\Delta t, t+\Delta t) - g_i(x,t) = \frac{\Delta t}{\tau_{\mathrm{D}}}[g_i^{\mathrm{eq}}(x,t) - g_i(x,t)]$$

for the temperature field (2)

where $\dot{J}_i$ is the momentum input from the buoyant body force, τ_v and τ_{D} are the relaxation time for flow and temperature LB equations, respectively, and $c_{\mathrm{s}} = c/\sqrt{3}$ is the speed of sound. The kinetic viscosity v and the thermal diffusivity α are given by their own relaxation time: $v = c_{\mathrm{s}}^2(\tau_v - 1/2)$ and $\alpha = c_{\mathrm{s}}^2(\tau_{\mathrm{D}} - 1/2)$. Furthermore, the local equilibrium distributions are given by [23]

$$f_i^{\mathrm{eq}}(x,t) = w_i\rho\left[1 + \frac{c_{iA}\cdot u_A}{c_{\mathrm{s}}^2} + \frac{u_A u_B}{2c_{\mathrm{s}}^2}\left(\frac{c_{iA}c_{iB}}{c_{\mathrm{s}}^2} - \delta_{AB}\right)\right]$$

for the flow field (3)

$$g_i^{\mathrm{eq}}(x,t) = w_i\theta\left[1 + \frac{c_{iA}\cdot u_A}{c_{\mathrm{s}}^2} + \frac{u_A u_B}{2c_{\mathrm{s}}^2}\left(\frac{c_{iA}c_{iB}}{c_{\mathrm{s}}^2} - \delta_{AB}\right)\right]$$

for the temperature field (4)

In these expressions, the flow properties are defined as

$$\text{Flowdensity:}\quad \rho = \sum_i f_i \tag{5}$$

$$\text{Momentumflux:}\quad \rho u_A = \sum_{iA} f_i c_{iA} \tag{6}$$

$$\text{Temperature (or concentration) population:}\quad \theta = \sum_i g_i \tag{7}$$

The subindices A and B are the components of Cartesian coordinates with implied summation for repeated indices. Furthermore, w_i is the weighting which can be determined to achieve isotropy of fourth-order tensor of velocities and Galilean invariance [23]. Using the Chapman–Enskog expansion, the continuity equation and the Navier–Stokes equations can be recovered exactly at the second-order approximation from the LB equation of the flow field, Eq. (1), without the additional body force term $\dot{J}_i$, as derived in [24]

$$\frac{\partial\rho}{\partial t} + \nabla\cdot(\rho\mathbf{u}) = 0 \tag{8}$$

$$\frac{\partial(\rho\mathbf{u}_A)}{\partial t} + \nabla_A\cdot(\rho\mathbf{u}_A\mathbf{u}_B) = -\nabla_A\left(c_{\mathrm{s}}^2\rho\right) + v\nabla_B\cdot(\nabla_A\rho\mathbf{u}_B + \nabla_B\rho\mathbf{u}_A) \tag{9}$$

Similarly, the convective–diffusive equation can be obtained from the LB equation of the temperature field, i.e. Eq. (2), as derived in [20,25]:

$$\frac{\partial\theta}{\partial t} + (\mathbf{u}\cdot\nabla)\theta = \nabla\cdot(\alpha\nabla\theta) \tag{10}$$

where θ denotes the temperature or concentration, and is replaced in the present study by the temperature T.

In simulating the natural convection problem, the additional buoyant body force term, $\dot{J}_i$, can be formulated by the Boussinesq approximation, i.e.

$$\dot{J}_i(x,t) = 3w_i\cdot g_y\cdot\beta\cdot[T(x,t) - T_\infty]\cdot\rho(x,t)\cdot c_{iy} \tag{11}$$

where g_y is the acceleration of gravity in the y-direction, β is the thermal expansion coefficient and is defined by $\beta \equiv -1/\rho_{\mathrm{ref}}(\partial\rho/\partial T)_P$ based on the reference density of the fluid ρ_{ref}, and c_{iy} is the y-component of c_i. Note that Eq. (11) only describes the buoyant effect acting on the y-direction of the lattice links. The terms $\rho(x,t)$ and $T(x,t)$, which are the dimensionless local density and temperature, are calculated at each lattice site using Eqs. (5) and (7), respectively. However, the temperature difference is normalized to the dimensionless format by setting $\Delta T \equiv T_{\mathrm{Boundary}} - T_\infty = 1$ as a constant and specifying $T_\infty = 0$ (the lowest reference temperature within the computational domain), such that $\Delta T = T(x,t)$ at each lattice site. Eq. (11) can then be simplified to

$$\dot{J}_i = 3w_i\cdot g_y\cdot\beta\cdot T(x,t)\cdot\rho(x,t)\cdot c_{iy} \tag{12}$$

This body force term does not contribute to the density of the flow but it does change the momentum of the flow as a result of the buoyancy. Additionally, the body force term, i.e. Eq. (12), maintains the term of local density $\rho(x,t)$ to prevent an over- or insufficient-variation of the local density when the local density is simplified as a fixed constant for incompressible applications. According to previous investigation [20], the current simple thermal LB model is applicable to incompressible thermal flows with negligible viscous dissipation. More details of this simplified LB model, including the Chapman–Enskog expansion and validation for natural convection problems, can be found in [20].

To simulate the natural convection problems by LBM, once the characteristic velocity $\left(V \equiv \sqrt{\beta g_y \Delta T H}\right)$ is determined, the kinetic viscosity (v) and thermal conductivity (α) can be obtained through the relation for the Prandtl number and Rayleigh number:

$$v^2 = \frac{V^2\ell^2 Pr}{Ra} \tag{13}$$

and

$$\alpha = \frac{v}{Pr} \tag{14}$$

where Ra is the Rayleigh number, Pr is the Prandtl number, and ℓ denotes the length scale according to the specific case of the natural convection problems. Hence, the relaxation time, τ_v and τ_{D}, for flow and temperature LB equations, i.e. Eqs. (1) and (2), can be determined, while the limitation of $0.5 < \tau$ for both relaxation times should be satisfied. It implies that both the kinetic viscosity (v) and thermal conductivity (α) cannot be fixed as constants in LBM simulations. The same approach to determine the flow parameters

for LBM computations in natural convection was also proposed in [16–19].

The present simulations use the D2Q9 model, i.e. two-dimensional nine-velocities model, and hence the relative weightings for Eqs. (3), (4), (11) and (12) are given by: $w_i = 4/9$ for $|c_i| = 0$ (for the static particle), $w_i = 1/9$ for $|c_i| = 1$, and $w_i = 1/36$ for $|c_i| = \sqrt{2}$. Regarding the boundary conditions of the flow field, the bounce-back scheme is applied for the no-slip solid walls. This scheme specifies the outgoing directions of the distribution function as the reverse of the incoming directions at the boundary sites. Regarding the temperature field, since the local temperature is defined as $T(x,y) = \sum_i g_i(x,y)$ in Eq. (7) and the no-slip condition $(u_x = u_y = 0)$ is applied for all solid nodes, the adiabatic walls can be simplified by employing the bounce-back scheme for temperature distribution function g_i to make the "heat flux-free state" in each lattice direction for the specific nodes applying to the adiabatic boundary condition, i.e. $\dot{q}_i = \partial T_i/\partial x_i = (g_i - g_{-i})/\Delta x = 0$. Moreover, the walls with a constant temperature can be specified by the equilibrium distribution computed from Eq. (4).

2.2. Symmetry

At the onset of bifurcation to the secondary instability, the periodic unsteady flow is characterized as a wave traveling along the axes of the rolls alternately. This oscillatory flow has a symmetry-breaking structure of flow. Previous studies [6,7] utilized a discrete subgroup G of the total symmetry group of the system. In present study, this subgroup is used to identify the bifurcation of the flow structure. Subgroup G consists of four elements, i.e.:

$$G = \{Id, S_1, S_2, S_3\} \tag{15}$$

where Id is the identity of the trivial symmetry group, and the symmetries S_1, S_2, and S_3 are given by

$$S_1 : (x,y) \to (-x,y); \quad (u_x, u_y, T') \to (-u_x, u_y, T') \tag{16}$$

$$S_2 : (x,y) \to (-x + L/2, 1 - y); \quad (u_x, u_y, T') \to (-u_x, -u_y, -T') \tag{17}$$

$$S_3 : (x,y) \to (x + L/2, 1 - y); \quad (u_x, u_y, T') \to (u_x, -u_y, -T') \tag{18}$$

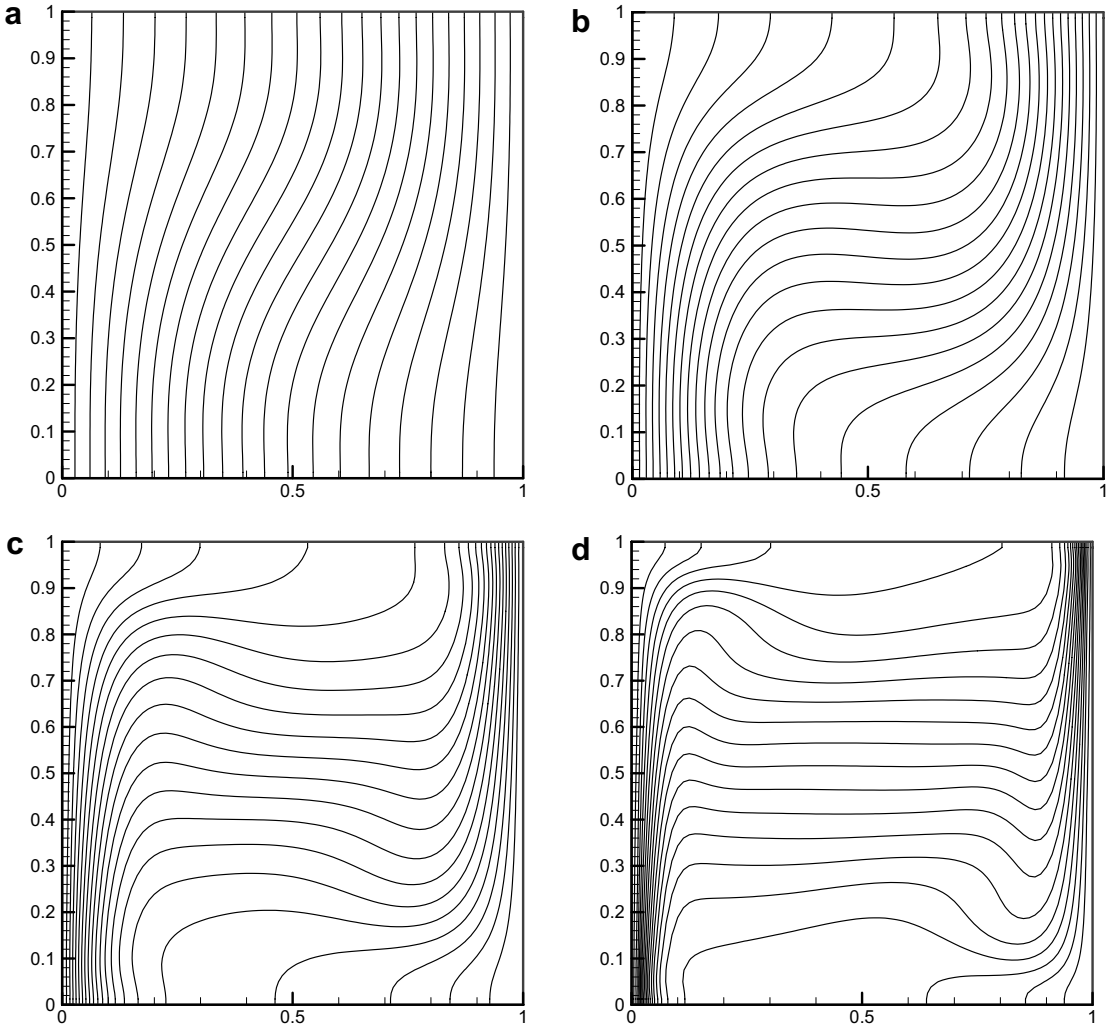

Fig. 1. Temperature contours for validation example of 2D square cavity with grid 81 × 81 at: (a) $Ra = 10^3$, (b) $Ra = 10^4$, (c) $Ra = 10^5$, and (d) $Ra = 10^6$.

where T' is the temperature deviation from the average temperature over the whole domain, and is defined as: $T' \equiv T(x,y) - \frac{(T_{\text{Bottom}} - T_{\text{Top}})}{2}$ for the simulations of Rayleigh–Bénard convection.

In the state of primary instability, the flow has the form of stationary rolls symmetric with respect to the full group G, i.e. Eq. (15). However, at the bifurcation to the secondary instability with a symmetry-breaking structure, three possible branches emerge with respect to which one bifurcating solution can be symmetric. These three branches correspond to subgroups $\{Id, S_1\}$, $\{Id, S_2\}$, and $\{Id, S_3\}$, respectively.

2.3. Frequency ratio

The present simulations define a dimensionless frequency ratio to quantify the oscillatory frequency for LBM applications. The dimensionless frequency ratio, f^*, is defined as

$$f^* \equiv \frac{f_D}{f_P} = \frac{\alpha \cdot t_p}{H^2} \tag{19}$$

where f_D is the reference thermal diffusive frequency, defined as $f_D = \frac{\alpha}{H^2}$, and f_P is the oscillatory frequency, i.e. $f_P = \frac{1}{t_p}$, in which t_p is time of period for the oscillatory flow. Note that f_P is the oscillatory frequency of flow induced by the thermal conduction. However, the reciprocal of the frequency ratio is the ratio of the diffusive time scale to the oscillatory time scale, i.e. $f^* = \frac{t_p}{t_D}$. Therefore, from Eq. (19), the frequency ratio is equal to zero for steady flows with stationary convection since the time of period is $t_p = 0$. Based on the definition of frequency ratio, the computed value of f^*, which is solved by LBM, could easily be applied to obtain the t_p for practical applications of engineering.

3. Validations of LB model using 2D square cavity

The simple thermal LB model in present study was validated by considering the case of natural convection in a 2D square cavity. In the simulations, the initial stationary flow was heated from the left wall of the cavity, i.e. $T_{\text{Left}} = 1$, while the right boundary was maintained at a constant low temperature, i.e. $T_{\text{right}} = 0$. The upper and bottom boundary walls were assigned to adiabatic boundary conditions. A vertical gravitational effect was applied in the y-direction. Regarding the flow field, the square cavity was assumed to be closed and the no-slip boundary condition was applied to each of the four solid walls. The initial conditions within the domain were specified as: $T(x,y) = 0$ and $u_x(x,y) = u_y(x,y) = 0$ with a uniform density of $\rho(x,y) = 1$.

In the simulations, the 2D cavity was mapped using a square lattice, in which $\Delta x = \Delta y$ for the D2Q9 model. The aspect ratio of the computational domain, i.e. $\text{AR} \equiv L/H$, was equal to 1. The simulations, including the grid-independence study, were performed using several different grid systems, i.e. 41×41, 81×81, and 161×161, respectively. The Prandtl number was assumed to be a fixed constant with a value of 0.71 and was defined as

$$Pr \equiv \frac{v}{\alpha} \tag{20}$$

In the simulations, the Rayleigh number (Ra) and the Nusselt number (Nu) were estimated to investigate the instability of the flow and the enhancement of the thermal transfer, respectively. The Ra and Nu were defined as

$$Ra = \frac{\beta \cdot \Delta T \cdot g_y \cdot L^3}{v\alpha} \tag{21}$$

and

$$Nu = 1 + \frac{\langle u_x \cdot T \rangle}{\alpha \cdot \Delta T / L} \tag{22}$$

where L is the horizontal length of the closed cavity, $\Delta T = 1$ is fixed and is the temperature difference between the left and right boundaries, and $\langle\,\rangle$ denotes the average value over the whole domain.

The simulations were performed at $Ra = 10^3$, 10^4, 10^5, and 10^6, respectively. The corresponding temperature

Table 1
Comparison of Nusselt numbers computed at different Rayleigh numbers using different grids with results presented in [28]

Ra	10^3	10^4	10^5	10^6
Nu by de Vahl Davis [28]	1.118	2.243	4.519	8.825
Nu by present LBM				
Grid: 41×41	1.105 (1.16%)	2.251 (0.37%)	4.551 (0.71%)	8.519 (3.47%)
Grid: 81×81	1.110 (0.72%)	2.249 (0.27%)	4.535 (0.35%)	8.734 (1.03%)
Grid: 161×161	1.113 (0.45%)	2.238 (0.22%)	4.508 (0.24%)	8.776 (0.56%)

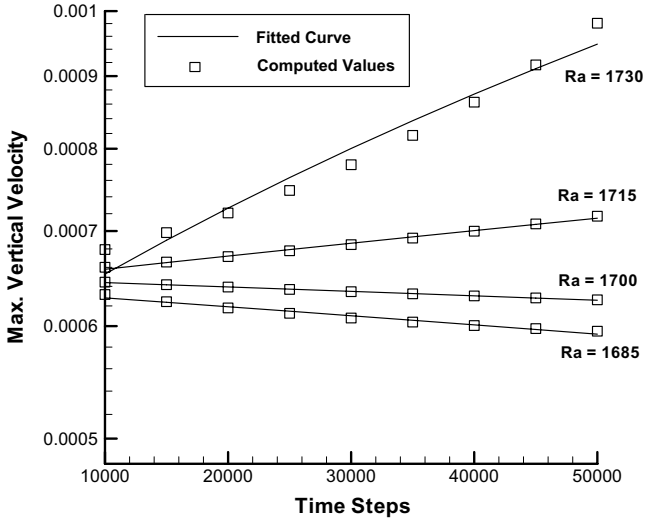

Fig. 2. Maximum vertical velocity growth/decay rate at different Rayleigh numbers for $V^2 = 0.085$ and $Pr = 0.71$.

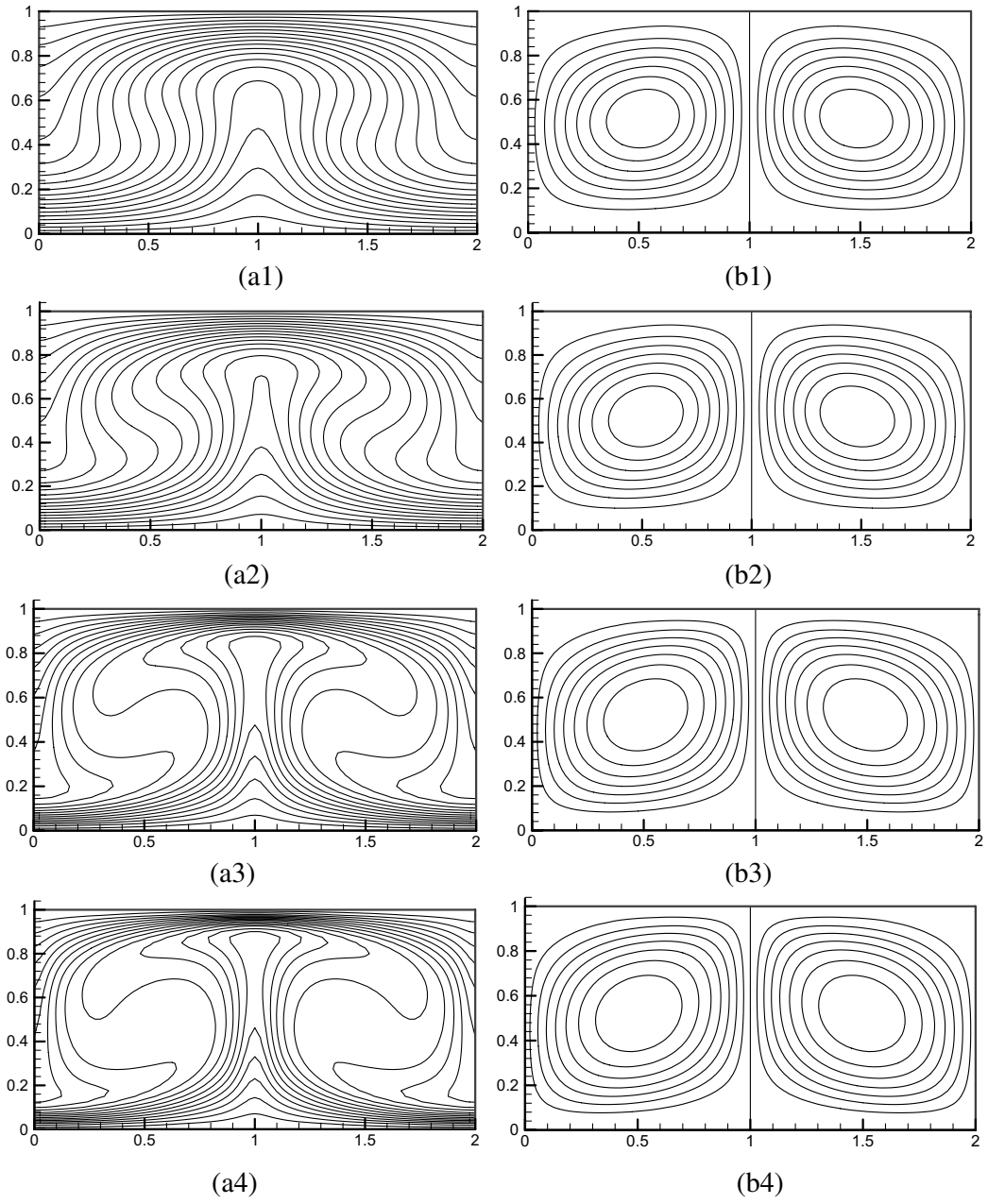

Fig. 3. Temperature and stream function contours at various Rayleigh numbers and $Pr = 0.71$: (a1) temperature contours at $Ra = 5000$, (a2) temperature contours at $Ra = 10,000$, (a3) temperature contours at $Ra = 50,000$, and (a4) temperature contours at $Ra = 10^5$; (b1) stream function contours at $Ra = 5000$, (b2) stream function contours at $Ra = 10,000$, (b3) stream function contours at $Ra = 50,000$, and (b4) stream function contours at $Ra = 10^5$.

contours are presented in Fig. 1. The current results are similar to those presented in [20,26,27]. Table 1 presents the simulated results obtained for the Nusselt number at Rayleigh numbers of $Ra = 10^3$, 10^4, 10^5, and 10^6, respectively, using each of three grid systems. The equivalent Nusselt data presented in [28] are also shown in Table 1 for comparison purposes. The percentage data given in parentheses indicate the deviation of the current simulation results from those given in [28]. It is observed that the results obtained using the current LB model are consistent with those reported in [28]. Using a grid size of 81×81 or 161×161, the discrepancy between the two sets of results is less than 1%. The maximum discrepancy is slightly larger than 1% when the coarse grid (41×41) is used.

4. Simulations of Rayleigh–Bénard convection

Rayleigh–Bénard convection is a flow driven by fluid expansion and gravity effects. In this natural convection problem, the initially static flow is heated from the bottom boundary, and a lower temperature is maintained at the upper wall. Additionally, a vertical gravitational force is applied to the y-direction of the computational domain. As the temperature difference between upper and bottom

boundaries is increased, the stationary conduction state becomes unstable by any small disturbance. According to linear stability theory, the critical wave number for Rayleigh–Bénard convection is $a_c = 3.117$. So that, the convective cells would be developed readily with an aspect ratio of $2\pi/a_c = 2.016$. An appropriate value of aspect ratio, $AR \equiv L/H = 2$, for simulations can be determined.

In the present Rayleigh–Bénard convection simulations, the computational 2D channel was mapped by the square lattice for D2Q9 model, comprising 81×41 grids. The same grid size was also applied to simulate the Rayleigh–Bénard convection using LBM or BGK based model at $Pr = 0.71$ in [17,18]. To compare the accuracy of the results obtained by present simple LB model with those using other LB models for the Rayleigh–Bénard convection at $Pr = 0.71$, we use the same mesh size (41×81). The side boundaries of the channel were assigned periodic boundary conditions for both the flow and the temperature fields. Meanwhile, the upper and bottom solid boundaries were assigned no-slip conditions for the flow field and were assigned constant temperatures of $T_{Upper} = 0$ and $T_{Bottom} = 1$, respectively, for the temperature field. A small perturbation in the form of a cosine wave with amplitude of 1×10^{-3} was applied to the density population. Note that a similar treatment for perturbation was applied to the density or to the temperature distribution functions as presented in [17,19,29].

In the present Rayleigh–Bénard convection simulations, the Prandtl number was defined as shown as in Eq. (20), but the definitions of the Rayleigh number and the Nusselt number were modified to

$$Ra = \frac{\beta \cdot \Delta T \cdot g_y \cdot H^3}{\nu\alpha} \tag{23}$$

and

$$Nu = 1 + \frac{\langle u_y \cdot T \rangle}{\alpha \cdot \Delta T/H} \tag{24}$$

where H is the vertical height of the channel, $\Delta T = 1$ is fixed and denotes the temperature difference between the upper and bottom boundaries.

The aim of the current simulations was to identify the oscillatory flows in 2D Rayleigh–Bénard convection. The simulations were performed for various value of the Prandtl number in the range of $0.71 \leqslant Pr \leqslant 70$, i.e. $Pr = 0.71$, 6, 25, and 70, respectively. Furthermore, the Rayleigh number was limited to the range $Ra \leqslant 10^5$. Under these conditions, the flow does not reach the fully developed turbulence regime, but bifurcations to oscillatory flows may occur at particular Prandtl numbers given an appropriate Rayleigh number. Importantly, since the simple LB model was used in incompressible limit, an appropriate characteristic velocity of natural convection, $V \equiv \sqrt{\beta g_y \Delta T H}$, was specified for each Prandtl number to ensure that incompressible conditions were achieved in each case.

4.1. A correction procedure for threshold of primary instability

According to linear stability theory, the primary instability of Rayleigh–Bénard convection with no-slip boundary conditions occurs at a critical Rayleigh number of $Ra_c = 1707.76$ with a wave number $a_c = 3.117$ [30]. Note that the values of Ra_c and a_c for primary instability are independent of the Prandtl number.

However, the fluids of LB are always compressible with the result that it bears potential danger [18]. Furthermore, as reported in [16,17,20], for the problem of natural convection using a thermal LBM, the characteristic velocity, $V \equiv \sqrt{\beta g_y \Delta T H}$, must be carefully determined to ensure that the compressible LB code can still be applied within the incompressible regime. The incompressible condition requires that the Mach number is $Ma \equiv U_{avg}/c_s \leqslant 0.1$, where the average macroscopic velocity U_{avg} can be estimated by the mean characteristic velocity, i.e. $U_{avg} \approx \sqrt{V^2_{mean}} = \sqrt{\beta g_y (T_{mean} - T_L) H}$. Unfortunately, there is no theoretical criterion to obtain the V value for various natural convection problems. Accordingly, before conducting the Rayleigh–Bénard convection simulations, this study examined the influence of the characteristic velocity (V) on the critical Rayleigh number (Ra_c) under various Prandtl numbers using this simple LB model.

To estimate the simulated critical Rayleigh number at different Prandtl numbers, the growth rate or decay rate of the maximum vertical velocity should be computed using a curve fitting technique at a slightly lower or slightly higher value of Rayleigh number than the theoretical critical Rayleigh number. In this study, Rayleigh numbers of $Ra = 1685$, 1700, 1715, and 1730 were specified. An interpolating scheme was then applied to determine the simulated critical Rayleigh number by the LB model. In

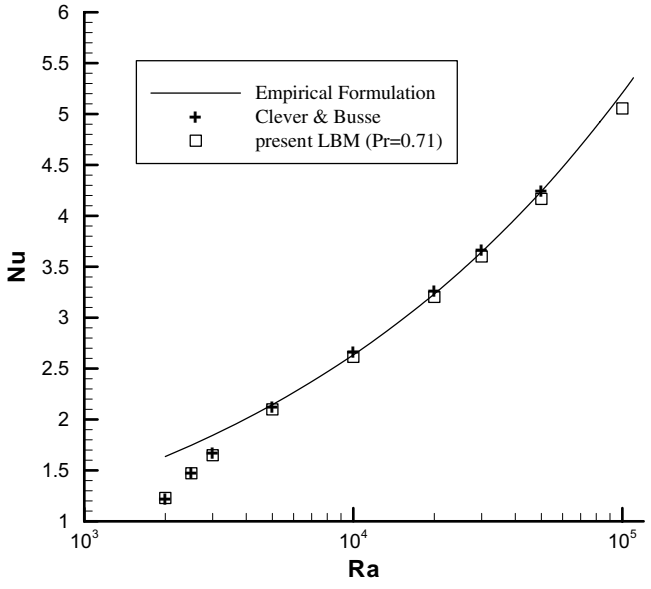

Fig. 4. Variation of Nusselt number with Rayleigh number at $Pr = 0.71$.

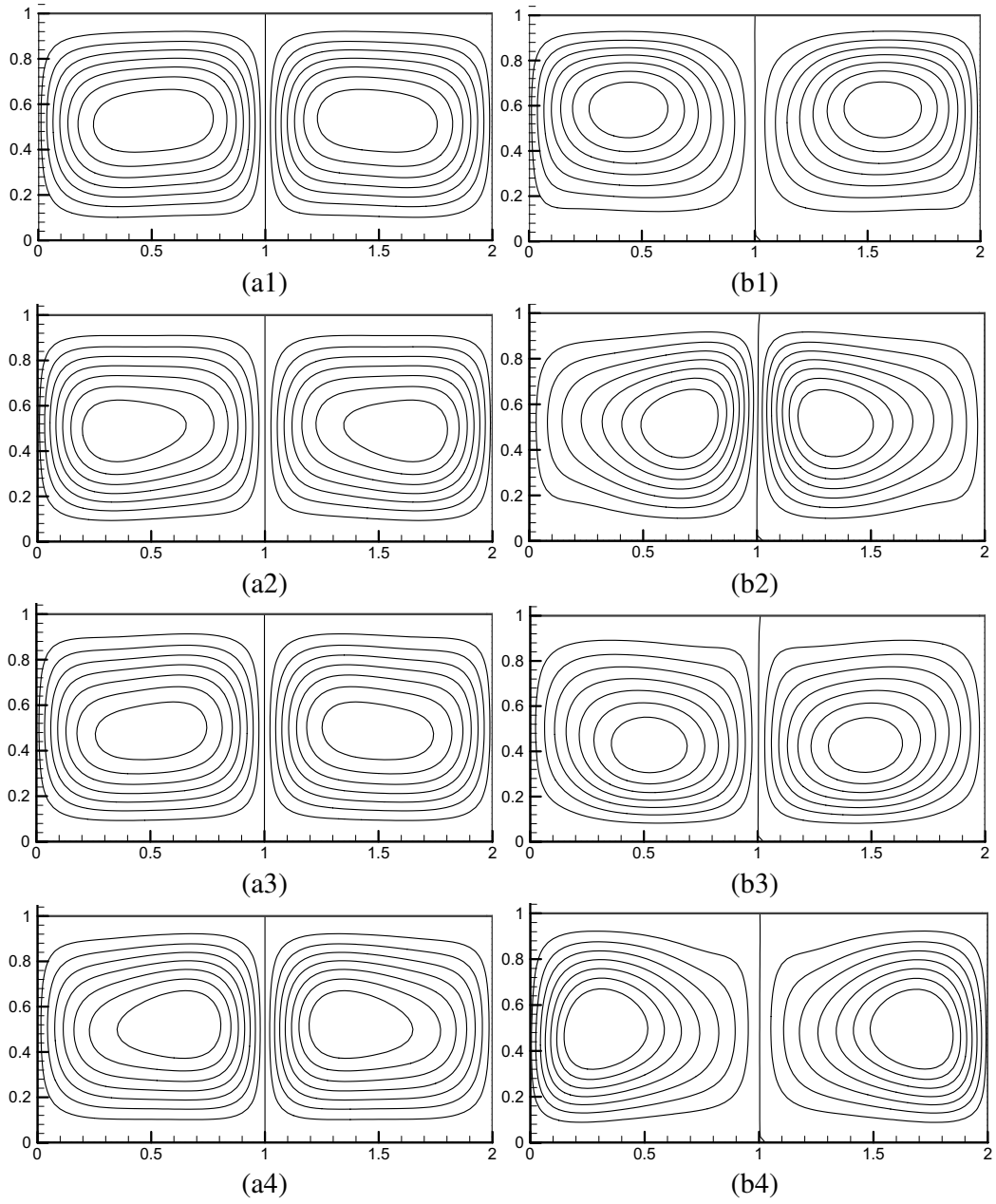

Fig. 5. Evolution of stream function contours in quarter-period steps at $Ra = 50{,}000$ and 10^5 for $Pr = 6$: (a1) $Ra = 50,000$ at $t = 0$, (a2) $Ra = 50,000$ at $t = t_p/4$, (a3) $Ra = 50,000$ at $t = t_p/2$, and (a4) $Ra = 50,000$ at $t = 3t_p/4$; (b1) $Ra = 10^5$ at $t = 0$, (b2) $Ra = 10^5$ at $t = t_p/4$, (b3) $Ra = 10^5$ at $t = t_p/2$, and (b4) $Ra = 10^5$ at $t = 3t_p/4$.

previous investigations, the squared value of the characteristic velocity, i.e. $V^2 = \beta g_y \Delta T H$, was specified as 0.1 in the case of $Pr = 0.71$ in [17], and in the case of $Pr = 1.0$ for a gas-kinetic BGK scheme presented in [18]. In the current study, several values of V^2 near 0.1, i.e. from 0.1 to 0.08, were tested for a Prandtl number of $Pr = 0.71$. The computed results indicated that the simulated critical Rayleigh number (Ra_c) varied from 1701.03 to 1721.88 in the velocity range $0.1 \leqslant V^2 \leqslant 0.08$. For a Prandtl number of $Pr = 0.71$, an optimum value of V^2 was found to be 0.085 for current LB model, and the associated critical Rayleigh number was $Ra_c = 1709.13$, i.e. a deviation of 0.34% from the theoretical value of 1707.76. Fig. 2 illustrates the maximum vertical velocity growth/decay rate at different Rayleigh numbers for the case of $V^2 = 0.085$ and $Pr = 0.71$. In simulations performed at different Prandtl numbers, the computed results for Ra_c were found to deviate significantly from the theoretical value of 1707.76 if the value of V^2 was maintained as a constant. In other words, the value of V^2 must be carefully chosen for different Prandtl numbers. Therefore, the present simulations employed the correction procedure to modify the value of V^2 for different Prandtl numbers in order to satisfy the correct theoretical value of $Ra_c = 1707.76$. By specifying a criteria that the deviation

of simulated Ra_c value from the theoretical Ra_c value should not be no more than 1% at each Prandtl number, it was determined that the appropriate value of V^2 were $V^2 = 0.035$ for $Pr = 6$, $V^2 = 0.014$ for $Pr = 25$, and $V^2 = 0.005$ for $Pr = 70$. An approximate analysis to explain this tendency is illustrated as follows. Consider a real case of the fixed Rayleigh number (i.e. $Ra_c = 1707.76$ for primary instability which is independent of Prandtl numbers) with increased Prandtl number, as an example of the fluid properties for air ($Pr = 0.71$, $\nu_{Air} = 1.5 \times 10^{-5}$ m^2/s at 20 °C) and for water ($Pr = 6.0$, $\nu_{Water} = 9.8 \times 10^{-7}$ m^2/s at 20 °C). Based on the relation in Eq. (13), the value of V^2 should be decreased as Prandtl number increasing to satisfy the fixed Rayleigh number. In the other words, larger Prandtl number requires smaller V^2 to lead a similar incompressible effect (similar value of Mach number) at same Rayleigh number because of the decreased kinetic viscosity.

4.2. Results obtained at Pr = 0.71

The first 2D Rayleigh–Bénard convection simulation considered the case of $Pr = 0.71$ with $V^2 = 0.085$. Fig. 3 presents the corresponding temperature and stream function contours at $Ra = 5000$, 10,000, 50,000, and 10^5. Meanwhile, Fig. 4 illustrates the variation of the Nusselt number with the Rayleigh number for $Ra = 2000$ to 10^5. For comparison purposes, Fig. 4 also presents the simulation results obtained by Clever and Busse [2] and those derived from the empirical formulation $Nu = 1.56(Ra/Ra_c)^{0.296}$. It can be seen that the values of the Nusselt number computed using the current LB model slightly deviate from those presented data in [2] at higher Rayleigh numbers ($Ra \geqslant 30,000$), and this conclusion by current LB model is similar to the simulation results obtained using the other LB models presented in [17,19] for the same Prandtl number of $Pr = 0.71$. Fig. 3 shows that no bifurcation to secondary instability occurs under the flow conditions considered in this particular simulation case, i.e. $Ra = 5000$, 10,000, 50,000, 10^5, and $Pr = 0.71$.

4.3. Results obtained at Pr = 6

For a Prandtl number of $Pr = 6$, V^2 was assigned a value of $V^2 = 0.035$ to ensure that the simulations were restricted to the incompressible regime. Additionally, a limitation of $Ra \leqslant 10^5$ was imposed to ensure numerical stability and computational accuracy.

The nonlinear bifurcated solutions at Prandtl numbers close to 6 have been investigated using non-Boltzmann based numerical models in previous studies. For 2D Rayleigh–Bénard convection with a stress-free boundary condition, Curry et al. [3] and Zienicke et al. [7] identified a transition from stationary convection to periodic convection at Rayleigh numbers between 30,000 and 31,000 in a computational domain with an aspect ratio of AR $= 2\sqrt{2}$ and a Prandtl number of $Pr = 6.8$. A periodic state of flow for the symmetry-breaking bifurcation from the stationary state was found at $Ra \sim 59,000$ by Prat et al. [6] for the case of convection in a domain with an aspect ratio of AR $= 2$ and $Pr = 10$ with a no-slip boundary condition. The authors also found that the profile of the stream function can be transformed into each other by applying the symmetries, S_2 and S_3, with shifted-time equal to half period. Furthermore, Stella and Bucchignani [8] identified an unsteady periodic flow at $Ra = 44,150 \pm 80$ in Rayleigh–Bénard convection at $Pr = 5.0$ with a no-slip boundary condition.

In the present simulations performed at $Pr = 6$, as the Rayleigh number was increased, a bifurcation solution with periodic frequency was found at $Ra \sim 48,000$. The simulation results showed that the flow below $Ra \sim 48,000$ was stationary convection, while that at higher

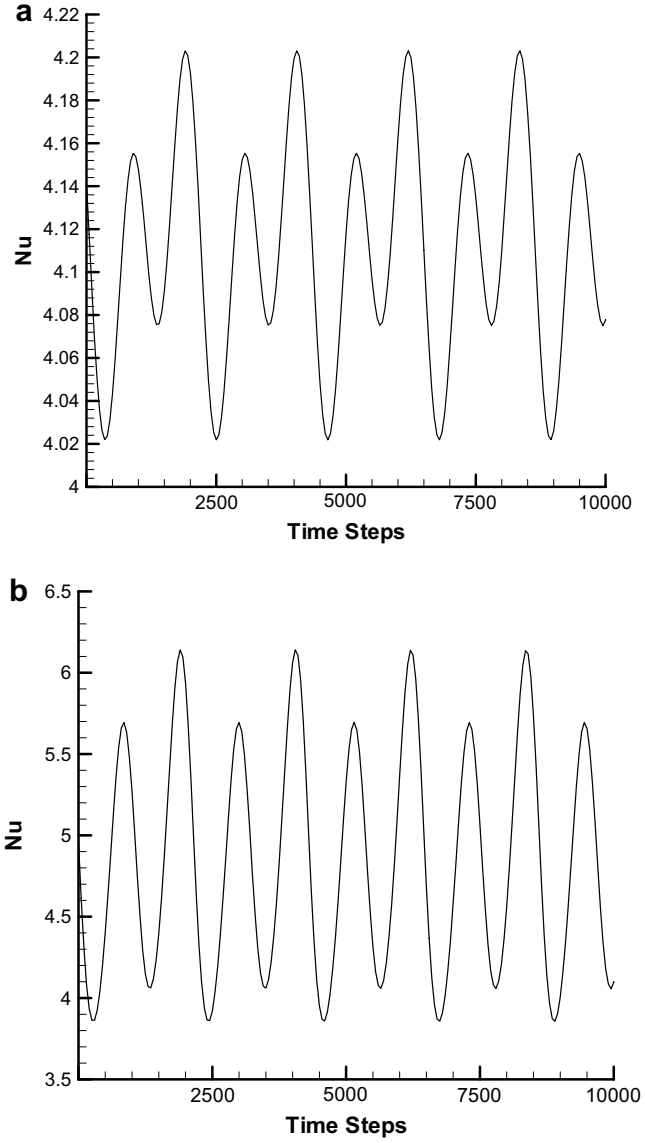

Fig. 6. Time history of Nusselt number at $Ra = 50,000$ and 10^5 for $Pr = 6$: (a) $Ra = 50,000$, and (b) $Ra = 10^5$.

Rayleigh numbers was oscillatory convection. This bifurcation solution broke symmetries S_2 and S_3, but symmetry S_1 was still maintained. The profile of the stream function contours can be transformed into each other by applying S_2 or S_3 at half period, i.e. at $t = 0$ and $t = t_p/2$ (or at $t = t_p/4$ and $t = 3t_p/4$) where t_p is the time of oscillatory period. Fig. 5 shows the evolution of the simulated stream function contours at $Ra = 50,000$ and 10^5, respectively, in quarter-period steps, i.e. at $t = 0$, $t = t_p/4$, $t = t_p/2$, and $t = 3t_p/4$. Fig. 6 shows the time history of the Nusselt number at $Ra = 50,000$ and 10^5, respectively, for the case of $Pr = 6$. It is observed that the periodic time steps of LBM (t_p) for $Ra = 50,000$ and 10^5 are around $t_p \sim 2150 \cdot \Delta t$, where Δt is the time interval of LBM. Therefore, the computed frequency ratios, as defined in Eq. (19), are obtained to be $f^* = 0.018$ and 0.013, respectively. It is observed that both the induced oscillatory frequency and the amplitude of the Nusselt number are increased at higher Rayleigh numbers. The trend is reported that the oscillatory flow moves more quickly as the Rayleigh number increasing. Finally, from Fig. 6, the average Nusselt numbers for $Ra = 50,000$ and 10^5 are estimated to be $\overline{Nu} = 4.118$ and 4.998, respectively.

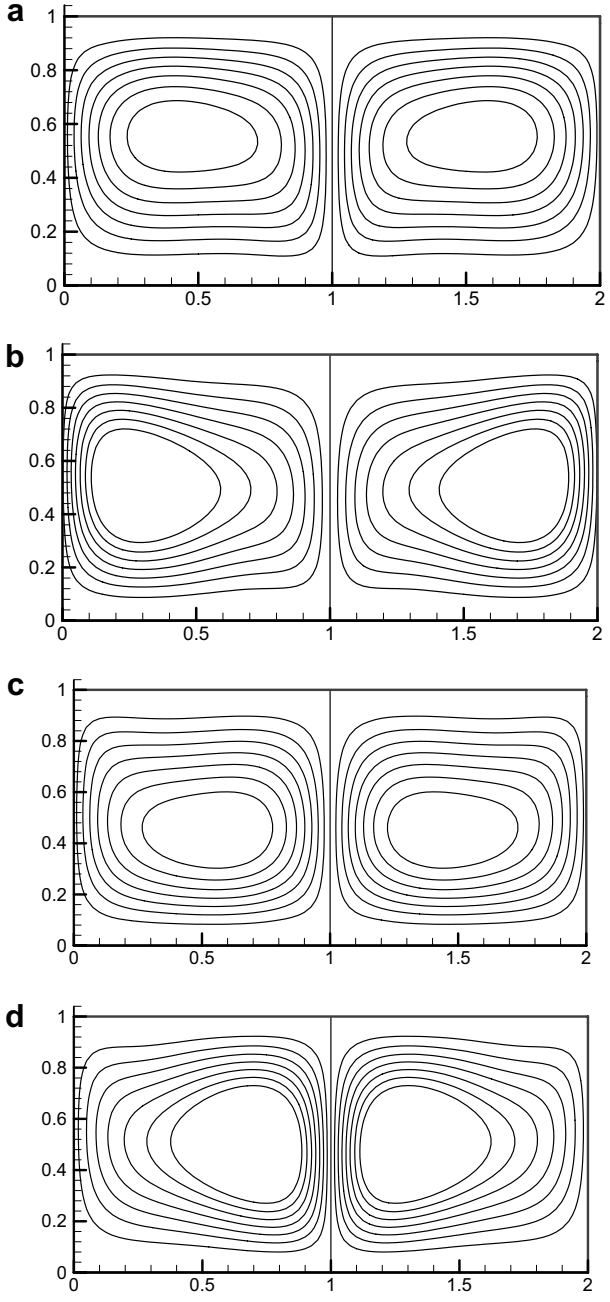

Fig. 7. Evolution of stream function contours in quarter-period steps at $Ra = 10^5$ and $Pr = 25$: (a) at $t = 0$, (b) at $t = t_p/4$, (c) at $t = t_p/2$, and (d) at $t = 3t_p/4$.

4.4. Results obtained at $Pr = 25$

For the simulations performed at $Pr = 25$, V^2 was assigned a value of $V^2 = 0.014$ to ensure that the simulations were within the incompressible regime. The simulation results indicated a bifurcation solution with periodic frequency at $Ra \sim 76,000$. This value of the Rayleigh number for the secondary instability is much higher than that observed in the previous case at $Pr = 6$. Fig. 7 shows the evolution of the computed stream function contours at $Ra = 10^5$ in quarter-period steps. It is observed that the periodic unsteady flow at $Ra = 10^5$ breaks symmetries S_2 and S_3, but the S_1 is still preserved. The streamline profile can also be transformed each other by applying the symmetries S_2 or S_3 at half period. Fig. 8 shows the time history of the Nusselt number at $Ra = 10^5$. The periodic time and frequency ratio are found to be $t_p \sim 6400 \cdot \Delta t$ and $f^* = 0.012$, respectively. Additionally, the average Nusselt number is calculated to be $\overline{Nu} = 5.126$. The value of frequency ratio and amplitude of the Nusselt number are similar to those observed at $Pr = 6$ with $Ra = 10^5$, and it is concluded that; when secondary instability occurs, the effect of thermal transfer and induced oscillatory frequency are similar for different values of Prandtl numbers at the same value of

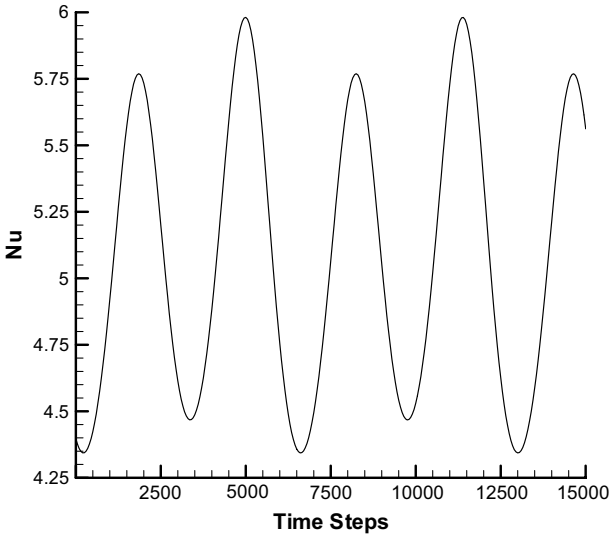

Fig. 8. Time history of Nusselt number at $Ra = 10^5$ for $Pr = 25$.

Rayleigh number. Finally, comparing the results obtained for $Pr = 6$ and $Pr = 25$, it is found that fluids with a higher Prandtl number have a wider stationary convection regime prior to bifurcation.

4.5. Results obtained at Pr = 70

For the simulations performed at $Pr = 70$, a value of $V^2 = 0.005$ was chosen to satisfy the incompressible condition. The simulation results indicated that no bifurcation to the oscillatory flow occurs at $Pr = 70$ with $Ra \leqslant 10^5$, i.e. only stationary convection takes place. Fig. 9 shows the stationary Rayleigh–Bénard convection at $Ra = 5000$, 10,000, 50,000, and 10^5, respectively. Comparing the simulation results obtained for $Pr = 0.71$ and 70, as shown in Figs. 3 and 9 sequentially, it is observed that neither sets of results indicate bifurcation to secondary instability. However, the stream function profiles and temperature contours at these two Prandtl numbers are very different. For the higher Prandtl number, i.e. $Pr = 70$, the flow momentum transports much faster than the thermal transfer, with the results that the streamline profile of the rolls is less inclined with a smaller velocity variation, as shown in Fig. 10, and a broader center of the rolls (cells).

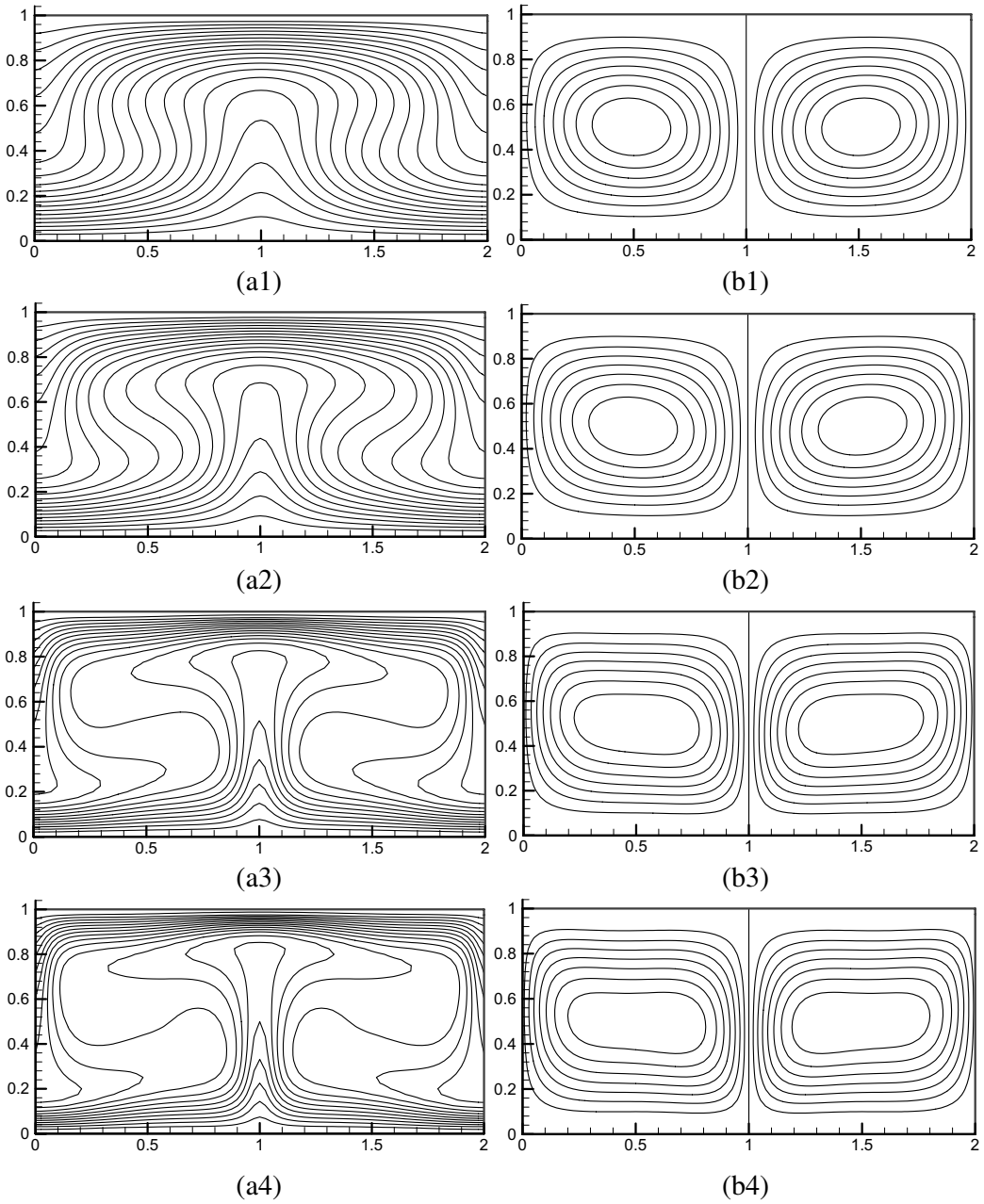

Fig. 9. Temperature and stream function contours at various Rayleigh numbers for $Pr = 70$: (a1) temperature contours at $Ra = 5000$, (a2) temperature contours at $Ra = 10,000$, (a3) temperature contours at $Ra = 50,000$, and (a4) temperature contours at $Ra = 10^5$; (b1) stream function contours at $Ra = 5000$, (b2) stream function contours at $Ra = 10,000$, (b3) stream function contours at $Ra = 50,000$, and (b4) stream function contours at $Ra = 10^5$.

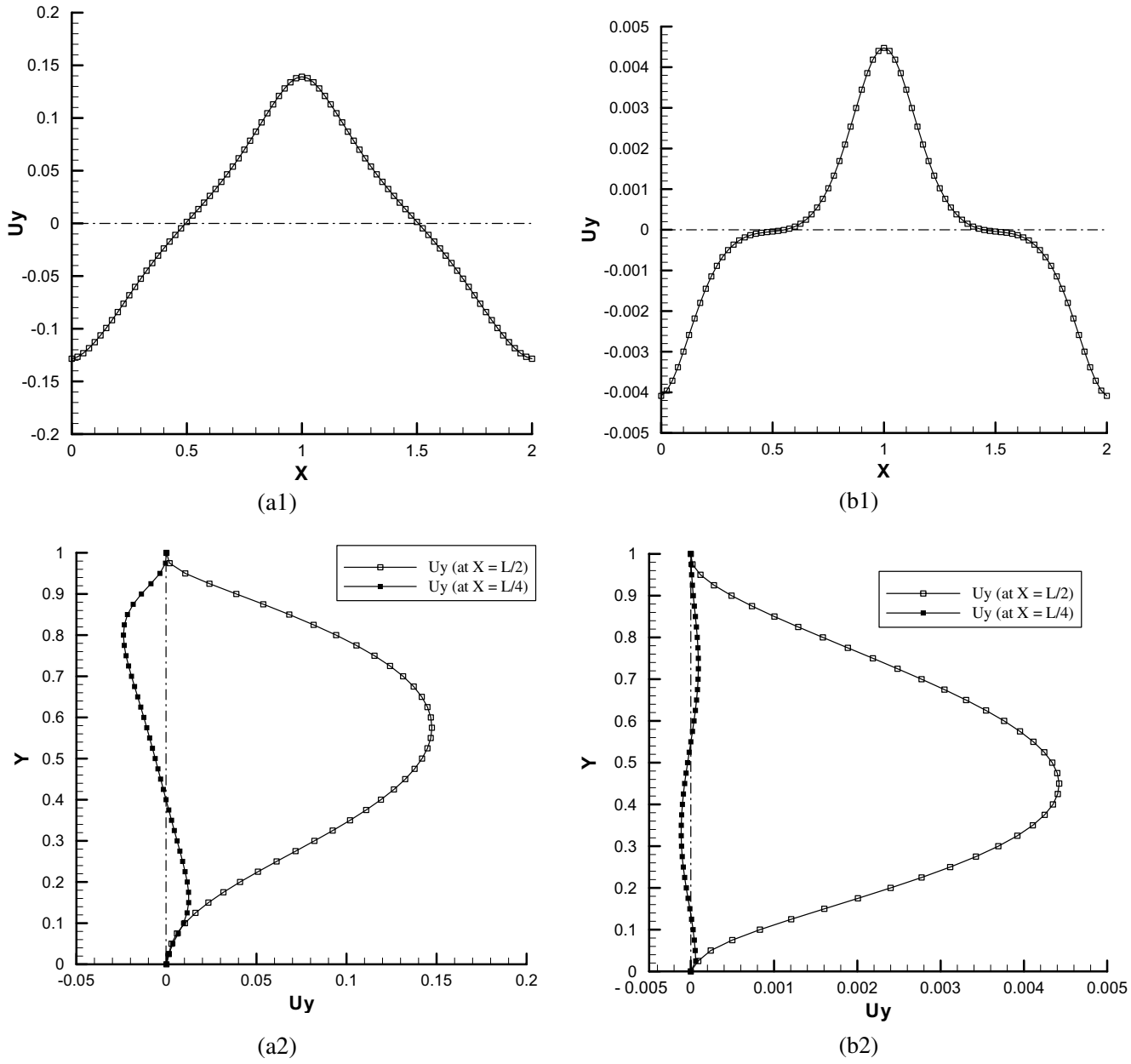

Fig. 10. Steady solutions of y-direction velocity component (U_y) profile against x-direction and y-direction at $Ra = 50,000$ for: (a1) $Pr = 0.71$ at $y = H/2$, (a2) $Pr = 0.71$ at $x = L/2$ and $x = L/4$, (b1) $Pr = 70$ at $y = H/2$, and (b2) $Pr = 70$ at $x = L/2$ and $x = L/4$.

4.6. Relationship between Nusselt number and Rayleigh number

In natural convection, the Nusselt number is a function of the Rayleigh number, the Prandtl number, and the aspect ratio. However, in the present simulations, the 2D Rayleigh–Bénard convection take place in a channel with an infinite horizontal length, such that a periodic boundary condition is imposed on the side boundaries. Therefore, the influence of the aspect ratio on the Nusselt number can be neglected.

Previous experimental and numerical investigations of the Nusselt number in Rayleigh–Bénard convection showed that the Nusselt number and the Rayleigh number are related by a power law: $Nu \propto Ra^r$, in which the power value r varies widely in the range of 0.20–0.386, but generally has a value of slightly less than 0.3. Fig. 11 plots the variation of the Nusselt number with the Rayleigh number in the Prandtl number and Rayleigh number ranges considered in the present simulations, i.e. $0.71 \leqslant Pr \leqslant 70$ and $Ra \leqslant 10^5$. It is apparent that the Nusselt number is relatively insensitive to the Prandtl number in the present simulations. Fig. 11 also plots the best-fitted curve obtained using the power value $r = 2/7 \approx 0.286$ for the near turbulence regime of Rayleigh–Bénard convection. It is observed that the Nusselt numbers computed using the current LB

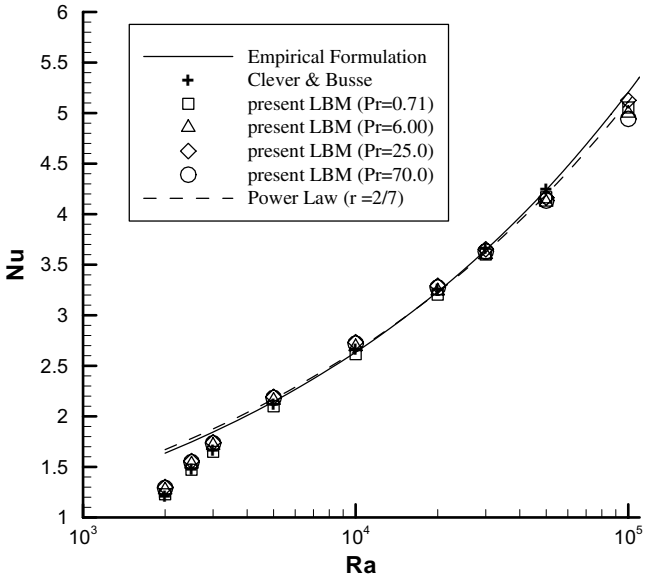

Fig. 11. Variation of Nusselt number with Rayleigh number for $0.71 \leqslant Pr \leqslant 70$ and $Ra \leqslant 10^5$.

model slightly deviate from the results by Clever and Busse [2] at higher values of the Rayleigh number. Similar results are obtained using others LB models to simulate the Rayleigh–Bénard convection [16–19]. For the incompressible limit, the Mach number ($Ma \equiv U_{\text{avg}}/c_s$) should be small. It requires that the characteristic velocity (V), which is a function of temperature difference ($\Delta T = T_H - T_L$), be small enough ($U_{\text{avg}} \approx \sqrt{V^2_{\text{mean}}} = \sqrt{\beta g_y (T_{\text{mean}} - T_L) H}$). In the buoyancy force, the mean temperature (T_{mean}) is taken as the reference temperature. Therefore, the LBM usually requires the smaller temperature difference. In present study, the Mach number is estimated by $Ma = \langle u_y \rangle / c_s$ at $Ra = 10^5$ and $Ra = 10^4$ respectively in the range of $0.71 \leqslant Pr \leqslant 70$. The results exhibited that the Mach numbers, which are in the order around 10^{-3}, become larger at higher Rayleigh number ($Ra = 10^5$) than those (Ma) at $Ra = 10^4$. The compressible effects are expected to exhibit in the flow field at higher Rayleigh number in Rayleigh–Bénard convection problems. Hence, the simulated results by presented LB model would be a little bit away from the experimental data.

5. Conclusions

This study performed a series of simulations of 2D Rayleigh–Bénard convection in the Prandtl number range $0.71 \leqslant Pr \leqslant 70$ and at Rayleigh numbers of $Ra \leqslant 10^5$ using a simple thermal LB model which neglects viscous thermal dissipation. In the simulations, the characteristic velocity V was carefully chosen for each Prandtl number using a correction procedure, as exhibited in Section 4.1, to ensure that the compressible LB method satisfies the incompressible limit. The simulation results have shown that in 2D Rayleigh–Bénard convection, bifurcation to secondary instability takes place at certain Prandtl numbers with an appropriate Rayleigh number, namely $Ra \sim 48{,}000$ for $Pr = 6$ and $Ra \sim 76{,}000$ for $Pr = 25$. However, the bifurcations are not observed for Prandtl numbers of $Pr = 0.71$ and $Pr = 70$. Bifurcations with a symmetry-breaking flow structure with single-frequency period oscillation have been observed. These bifurcation solutions are strongly dependent on fluid properties (i.e. the Prandtl numbers), and these simulations results are in good qualitative agreement with those identified experimentally by Krishnamurti [5] and numerically by Prat [6].

The employed LB model is very simple to simulate the problems of Rayleigh–Bénard instability. The present study provides more details of the Rayleigh–Bénard instability from threshold of primary instability to periodic oscillatory regime (secondary instability) within the range of $0.71 < Pr < 70$. The simulation results confirm the suitability of the current simplified LB model for simulating the bifurcation to secondary instability near the turbulent regime in the 2D Rayleigh–Bénard convection problem while the compressible effect of the LB model is taken into account. Unfortunately, there is no available criterion to choose the appropriated V value presented previously in LBM for natural convection simulations. A further study of theoretical formulation based on the kinetic theory is essential to investigate the instability problem of natural convection, and this is our current task.

The solutions for the Nusselt numbers computed using the current LB model slightly deviate from the results by Clever and Busse [2] at higher values of the Rayleigh number, i.e. $Ra \geqslant 30{,}000$. The information for incompressible limit at higher Rayleigh number was provided in Section 4.6.

Furthermore, flow with two-frequency quasi-periodic oscillation has not been observed in present simulations. To overcome the drawbacks or difficulties of the present LB model for simulating flows with higher Rayleigh numbers or in the fully turbulent regime, the future studies to develop a robust thermal LB model which takes into account the effect of viscous thermal dissipation and applies an appropriated turbulent model are required.

References

[1] S. Chandrasekhar, Hydrodynamic and Hydromagnetic Stability, Clarendon Press, Oxford, 1961.
[2] R.M. Clever, F.H. Busse, Transition to time-dependent convection, J. Fluid Mech. 65 (4) (1974) 625–645.
[3] J.H. Curry, J.R. Herring, J. Loncaric, S.A. Orszag, Order and disorder in two- and three-dimensional Bénard convection, J. Fluid Mech. 147 (1984) 1–38.
[4] R.E. Ecke, H. Haucke, Y. Maeno, J.C. Wheatley, Critical dynamics at a Hopf bifurcation to oscillatory Rayleigh–Bénard convection, Phys. Rev. A 33 (3) (1986) 1870.
[5] R. Krishnamurti, Some further studies on the transition to turbulent convection, J. Fluid Mech. 60 (1973) 285–303.
[6] J. Prat, J.M. Massaguer, I. Mercader, Large-scale flows and resonances in 2-D thermal convection, Phys. Fluids 7 (1) (1995) 121–134.

[7] E. Zienicke, N. Seehafer, F. Feudel, Bifurcations in two-dimensional Rayleigh–Bénard convection, Phys. Rev. E 57 (1) (1998) 428–435.
[8] F. Stella, E. Bucchignani, Rayleigh–Bénard convection in limited domains: part 1 – oscillatory flow, Numer. Heat Transfer Part A 36 (1) (1999) 1–16.
[9] E. Bucchignani, F. Stella, Rayleigh–Bénard convection in limited domains: part 2 – transition to chaos, Numer. Heat Transfer Part A 36 (1) (1999) 17–34.
[10] P.Y. Tzeng, M.H. Liu, Direct-simulation Monte Carlo modeling on two-dimensional Rayleigh–Bénard instabilities of rarefied gas, Numer. Heat Transfer Part A 47 (8) (2005) 805–823.
[11] S. Chen, G.D. Doolen, Lattice Boltzmann method for fluid flows, Annu. Rev. Fluid Mech. 30 (1998) 329–364.
[12] Y.G. Lai, C.L. Lin, J. Huang, Accuracy and efficiency study of lattice Boltzmann method for steady-state flow simulations, Numer. Heat Transfer Part B 39 (1) (2001) 21–43.
[13] D. Yu, R. Mei, L.S. Luo, W. Shyy, Viscous flow computations with the method of lattice Boltzmann equation, Progr. Aerospace Sci. 39 (2003) 329–367.
[14] D. Raabe, Overview of the lattice Boltzmann method for nano- and microscale fluid dynamics in materials science and engineering, Model. Simul. Mater. Sci. Eng. 12 (2004) R13–R46.
[15] S. Succi, The Lattice Boltzmann Equation for Fluid Dynamics and Beyond, Clarendon Press, Oxford, 2001.
[16] X. Shan, Simulation of Rayleigh–Bénard convection using a lattice Boltzmann method, Phys. Rev. E 55 (3) (1997) 2780–2788.
[17] X. He, S. Chen, G.D. Doolen, A novel thermal model for the lattice Boltzmann method in incompressible limit, J. Comput. Phys. 146 (1998) 282–300.
[18] K. Xu, S.H. Lui, Rayleigh–Bénard simulation using the gas-kinetic Bhatnagar–Gross–Krook scheme in the incompressible limit, Phys. Rev. E 60 (1) (1999) 464–470.
[19] T. Inamuro, M. Yoshino, H. Inoue, R. Mizuno, F. Ogino, A lattice Boltzmann method for a binary miscible fluid mixture and its application to a heat-transfer problem, J. Comput. Phys. 179 (2002) 201–215.
[20] Y. Peng, C. Shu, Y.T. Chew, Simplified thermal lattice Boltzmann model for incompressible thermal flows, Phys. Rev. E 68 (026701) (2003) 1–8.
[21] H. Yu, L.S. Luo, S.S. Girimaji, Scalar mixing and chemical reaction simulations using lattice Boltzmann method, Int. J. Comp. Eng. Sci. 3 (1) (2002) 73–87.
[22] G. Barrios, R. Rechtman, J. Rojas, R. Tovar, The lattice Boltzmann equation for natural convection in a two-dimensional cavity with a partially heated wall, J. Fluid Mech. 522 (2005) 91–100.
[23] Y.H. Qian, D. d'Humieres, P. Lallemand, Lattice BGK models for Navier–Stokes equation, Europhys. Lett. 17 (6) (1992) 479–484.
[24] Y.H. Qian, S.A. Orszag, Lattice BGK models for the Navier–Stokes equation: non-linear deviation in compressible regimes, Europhys. Lett. 21 (1993) 255–259.
[25] S.P. Dawson, S. Chen, G.D. Doolen, Lattice Boltzmann computations for reaction-diffusion equations, J. Chem. Phys. 98 (1993) 1514–1523.
[26] Y. Peng, C. Shu, Y.T. Chew, A 3D incompressible thermal lattice Boltzmann model and its application to simulate natural convection in a cubic cavity, J. Comput. Phys. 193 (2003) 260–274.
[27] E.J. Braga, M.J.S. de Lemos, Heat transfer in encloses having a fixed amount of solid material simulated with heterogeneous and homogeneous models, Int. J. Heat Mass Transfer 48 (2005) 4748–4765.
[28] G. de Vahl Davis, Natural convection of air in a square cavity, a bench mark numerical solution, Int. J. Numer. Meth. Fluids 3 (1983) 249–264.
[29] Y. Zhou, R. Zhang, I. Staroselsky, H. Chen, Numerical simulation of laminar and turbulent buoyancy-driven flows using a lattice Boltzmann based algorithm, Int. J. Heat Mass Transfer 47 (2004) 4869–4879.
[30] W.H. Reid, D.L. Harris, Some further results in the Bénard problem, Phys. Fluids 1 (1958) 102.